Frequency domain elastic FWI for VTI media

Junxiao Li, Kris Innanen, Wenyong Pan, Geng Yu

ABSTRACT

In this study, a frequency-domain elastic full waveform inversion algorithm for 2-D VTI media has been developed. The forward problem used in this inversion algorithm is simulated by applying frequency domain finite difference method, which is a fast approach for multi-source and multi-receiver acquisition. For the anisotropic inversion of VTI media, five elastic constants (c_{11}, c_{13}, c_{33}, c_{44} and density) have to be dealt with. In this paper, the gradients of four elastic constants are calculated in matrix forms. To accelerate the convergence rate of inversion, the pusdo-Hessian is also implemented in the objective function. The inversion results in the paper show that parameters c_{11}, c_{13} and c_{33} can be inverted properly, yet the inversion result of c_{44} is not satisfying.

INTRODUCTION

In oil and gas exploration, seismic inversion plays a key role in delineating subsurface structures (Tarantola, 1984; Pratt et al., 1998; Shin and Min, 2006). Most of the FWI techniques are performed under the assumption that the underground formations are isotropic, yet, according to Thomsen (1986), shale, laminated thin-layers and oriented vertical fractures are transversely isotropic (TI) media. And transversely isotropic media with a vertical symmetry axis (VTI) are commonly observed in sedimentary formations. For this reason, anisotropy should be taken into account in FWI.

In the anisotropic waveform inversion, more formation parameters should be inverted than in isotropic inversion (Chang and McMechan, 2009; Kamath and Tsvankin, 2016; Pan et al., 2016). This implies multiparameter anisotropic elastic FWI is a highly non-linear problem. Plessix (2009) proposed that the inversion resolution can be greatly enhanced by taking anisotropy into consideration. Barnes et al. (2008) used the full waveform inversion in transversely isotropic media. In his paper, the Thomsen parameters (Thomsen, 1986)(including isotropic parameters of vertical P- and S-wave velocities, anisotropic parameters of δ and ε) are inverted. It showed that the isotropic parameters can be reconstructed properly yet the anisotropic parameters can not be well restored. According to Gholami and Siahkoohi (2010), Thomson's parameters can not be inverted simultaneously even if source-receiver stations are well distributed at all directions. Gholami et al. (2013) also pointed out that the choice of parameterization is important for anisotropic FWI. Lee et al. (2010) applied a frequency-selection strategy, moving from lower to higher frequencies to invert elastic constants(c_{11}, c_{13}, c_{33}, c_{44}) in VTI meida. In his paper, he coupled elastic constants c_{11} and c_{33} based on Thomsen's relstionship. And the steepest-descent method based on the adjoint state of the wave equations (Lailly, 1983; Tarantola, 1984; Pratt et al., 1998) are used to updated by model parameters. In this paper, we will invert elastic constants c_{11}, c_{13}, c_{33}, c_{44} while keeping density fixed. As an inversion problem, FWI requires intensive computation. An efficient step-length formula is extremely important to accelerate the convergence rate. In this study, we estimate the step length by a modified quadratic interpolation method. The inversion results show that satisfying reconstruction can be obtained

for elastic constants c_{11}, c_{33} and c_{13}, yet the inversion of c_{44} needs to be enhanced.

FREQUENCY DOMAIN FORWARD MODELING

Wave propagation in an elastic medium is governed by the equation:

$$\rho\partial_t^2 u_j = \sigma_{ij,j}, \tag{1}$$

where $i, j = 1, 2, 3$, ρ is the density, u_i is the displacement vector and σ_{ij} is stress tensor, and where $\sigma_{ij,j}$ represent spatial derivatives of the stress tensor. The comma between subscripts is used for spatial derivatives. The summation convention for repeated subscripts is assumed. According to Hooke's law, the relationship between the stress and strain tensors is,

$$\sigma_{ij} = c_{ijkl}\varepsilon_{kl}, \tag{2}$$

where c_{ijkl} are the elastic stiffness coefficients. The strain tensor ε_{kl} is

$$\varepsilon_{kl} = \frac{1}{2}(u_{k,l} + u_{l,k}). \tag{3}$$

In the case of a transverse isotopic medium, the second-order wave equation system in frequency domain can be written as

$$\begin{aligned} -\rho\omega^2 u_x &= \tfrac{\partial\sigma_{11}}{\partial x} + \tfrac{\partial\sigma_{12}}{\partial y} + \tfrac{\partial\sigma_{13}}{\partial z} + f_x \\ -\rho\omega^2 u_y &= \tfrac{\partial\sigma_{21}}{\partial x} + \tfrac{\partial\sigma_{22}}{\partial y} + \tfrac{\partial\sigma_{23}}{\partial z} + f_y \\ -\rho\omega^2 u_z &= \tfrac{\partial\sigma_{31}}{\partial x} + \tfrac{\partial\sigma_{32}}{\partial y} + \tfrac{\partial\sigma_{33}}{\partial z} + f_z \end{aligned} . \tag{4}$$

For formations with a vertical symmetry axis (VTI), the elastic stiffness tensor is

$$c_{VTI} = \begin{bmatrix} c_{11} & c_{11}-2c_{66} & c_{13} & 0 & 0 & 0 \\ c_{11}-2c_{66} & c_{11} & c_{13} & 0 & 0 & 0 \\ c_{13} & c_{13} & c_{33} & 0 & 0 & 0 \\ 0 & 0 & 0 & c_{44} & 0 & 0 \\ 0 & 0 & 0 & 0 & c_{44} & 0 \\ 0 & 0 & 0 & 0 & 0 & c_{66} \end{bmatrix}, \tag{5}$$

And the 2D elastic stiffness tensor is reduced to

$$c_{VTI} = \begin{bmatrix} c_{11} & c_{13} & 0 \\ c_{13} & c_{33} & 0 \\ 0 & 0 & c_{44} \end{bmatrix}. \tag{6}$$

The 2D elastic wave equations for VTI media can be written as

$$
\begin{aligned}
-\rho\omega^2\tilde{u}_x &= \tfrac{\partial}{\partial x}\left(c_{11}\tfrac{\partial u_x}{\partial x} + c_{13}\tfrac{\partial u_z}{\partial z}\right) + \tfrac{\partial}{\partial z}\left(c_{44}\left(\tfrac{\partial u_x}{\partial z} + \tfrac{\partial u_z}{\partial x}\right)\right) + \tilde{f}_x(\omega) \\
-\rho\omega^2\tilde{u}_z &= \tfrac{\partial}{\partial z}\left(c_{13}\tfrac{\partial u_x}{\partial x} + c_{33}\tfrac{\partial u_z}{\partial z}\right) + \tfrac{\partial}{\partial x}\left(c_{44}\left(\tfrac{\partial u_x}{\partial z} + \tfrac{\partial u_z}{\partial x}\right)\right) + \tilde{f}_z(\omega).
\end{aligned} \tag{7}
$$

Employing the finite-element method, the above equations can be written as

$$
\mathbf{W}\tilde{\mathbf{u}} = \tilde{\mathbf{f}}. \tag{8}
$$

Rewrite the above equations into the matrix formalism (Pratt and Worthington, 1988), we have

$$
\begin{bmatrix} W_{xx}(\mathbf{x},\omega) & W_{xz}(\mathbf{x},\omega) \\ W_{zx}(\mathbf{x},\omega) & W_{zz}(\mathbf{x},\omega) \end{bmatrix} \begin{bmatrix} \tilde{u}_x(\mathbf{x},\omega) \\ \tilde{u}_z(\mathbf{x},\omega) \end{bmatrix} = \begin{bmatrix} \tilde{f}_x(\mathbf{x},\omega) \\ \tilde{f}_z(\mathbf{x},\omega) \end{bmatrix}, \tag{9}
$$

where, $\begin{bmatrix} \tilde{f}_x(\mathbf{x},\omega) & \tilde{f}_z(\mathbf{x},\omega) \end{bmatrix}^T$ is the source vector $\tilde{f}$, and the wave operator $W(\mathbf{x},\omega)$ is defined as

$$
W(\mathbf{x},\omega) = \begin{bmatrix} W_{xx}(\mathbf{x},\omega) & W_{xz}(\mathbf{x},\omega) \\ W_{zx}(\mathbf{x},\omega) & W_{zz}(\mathbf{x},\omega) \end{bmatrix}. \tag{10}
$$

In VTI media, $W(\mathbf{x},\omega)$ can be written as

$$
\begin{aligned}
W_{xx}(\mathbf{x},\omega) &= -\rho(\mathbf{x})\omega^2 - \tfrac{\partial}{\partial x}c_{11}\tfrac{\partial}{\partial x} - \tfrac{\partial}{\partial z}c_{44}\tfrac{\partial}{\partial z} \\
W_{xz}(\mathbf{x},\omega) &= -\tfrac{\partial}{\partial x}c_{13}\tfrac{\partial}{\partial z} - \tfrac{\partial}{\partial z}c_{44}\tfrac{\partial}{\partial x} \\
W_{zx}(\mathbf{x},\omega) &= -\tfrac{\partial}{\partial z}c_{13}\tfrac{\partial}{\partial x} - \tfrac{\partial}{\partial x}c_{44}\tfrac{\partial}{\partial z} \\
W_{zz}(\mathbf{x},\omega) &= -\rho(\mathbf{x})\omega^2 - \tfrac{\partial}{\partial z}c_{33}\tfrac{\partial}{\partial z} - \tfrac{\partial}{\partial x}c_{44}\tfrac{\partial}{\partial x}
\end{aligned} . \tag{11}
$$

In isotropic media, $W(\mathbf{x},\omega)$ can be written as

$$
\begin{aligned}
W_{xx}(\mathbf{x},\omega) &= -\rho(\mathbf{x})\omega^2 - \tfrac{\partial}{\partial x}\rho(\mathbf{x})V_p(\mathbf{x})^2\tfrac{\partial}{\partial x} - \tfrac{\partial}{\partial z}\rho(\mathbf{x})V_s(\mathbf{x})^2\tfrac{\partial}{\partial z} \\
W_{xz}(\mathbf{x},\omega) &= -\tfrac{\partial}{\partial x}(\rho(\mathbf{x})V_p(\mathbf{x})^2 - 2\rho(\mathbf{x})V_s(\mathbf{x})^2)\tfrac{\partial}{\partial z} - \tfrac{\partial}{\partial z}\rho(\mathbf{x})V_s(\mathbf{x})^2\tfrac{\partial}{\partial x} \\
W_{zx}(\mathbf{x},\omega) &= -\tfrac{\partial}{\partial z}\left(\rho(\mathbf{x})V_p(\mathbf{x})^2 - 2\rho(\mathbf{x})V_s(\mathbf{x})^2\right)\tfrac{\partial}{\partial x} - \tfrac{\partial}{\partial x}\rho(\mathbf{x})V_s(\mathbf{x})^2\tfrac{\partial}{\partial z} \\
W_{zz}(\mathbf{x},\omega) &= -\rho(\mathbf{x})\omega^2 - \tfrac{\partial}{\partial z}\rho(X\mathbf{x})V_p(\mathbf{x})^2\tfrac{\partial}{\partial z} - \tfrac{\partial}{\partial x}\rho(\mathbf{x})V_s(\mathbf{x})^2\tfrac{\partial}{\partial x}
\end{aligned} . \tag{12}
$$

GRADIENT DIRECTION

The main objective of FWI is to find a suitable velocity model by minimizing the objective function based on the residuals between modeled and field data (Lailly, 1983; Tarantola, 1984; Virieux and Operto, 2009). The general relation between the model **m** and the data **u** can be expressed as

$$
\mathbf{u} = g(\mathbf{m}). \tag{13}
$$

The objective function can be written as

$$E(\mathbf{m}) = \frac{1}{2}\sum_{\omega}\sum_{\mathbf{s}}\left[\mathbf{u}-\mathbf{d}\right]^{T}\left[\mathbf{u}-\mathbf{d}\right]^{*}. \tag{14}$$

where $\mathbf{u}$ and $\mathbf{d}$ are the modelled and observed data, superscripts T and $*$ are tranpose and complex conjugate, respectively. ω and $\mathbf{s}$ denote the frequency and source.

The inversion problem now has changed into finding the global minimum of this misfit function. We choose an initial model and perform iterations to reach its neighboring minimum. And then the best model calculated at one iteration can be treated as new initial model for the next iteration. For a given initial model $\mathbf{m}_0$, take a second-order Taylor-Lagrange expansion, the misfit funstion of equation (14) can be expressed as

$$E(\mathbf{m}_0+\delta\mathbf{m}) = E(\mathbf{m}_0) + \nabla_{\mathbf{m}}E(\mathbf{m}_0)^{T}\delta\mathbf{m} + 1/2\delta\mathbf{m}^{T}\nabla^{2}_{\mathbf{m}}E(\mathbf{m}_0)\delta\mathbf{m} + O(\delta\mathbf{m}^{2}), \tag{15}$$

where, $\delta\mathbf{m}$ is parameter perturbation and $O(\delta\mathbf{m}^2)$ is second-order Lagrange remainder, and $\nabla_{\mathbf{m}}E$ is the gradient.

When a local minimum of E is reached with a suitable increment of $\delta\mathbf{m}$, the above equation can be written as

$$\nabla_{\mathbf{m}}E(\mathbf{m}_0) = \nabla^{2}_{\mathbf{m}}E(\mathbf{m}_0)\delta\mathbf{m} = H(\mathbf{m}_0)\delta\mathbf{m}, \tag{16}$$

The derivative of the gradient with respect to model $\mathbf{m}$ is Hessian H. For a perturbation of the k^{th} parameter of a model m, its gradient can be obtained by taking the partial derivative of the objective function of equation (14) with respect to the k^{th} model parameter as

$$\nabla_{m_k}E(m_k) = \sum_{\omega}\sum_{\mathbf{s}} Re\left[\left(\frac{\partial\tilde{\mathbf{u}}}{\partial m_k}\right)^{T}\left(\tilde{\mathbf{u}}-\tilde{\mathbf{d}}\right)^{*}\right]. \tag{17}$$

The first term on the RHS of the above equation can be obtained by taking the partial derivative of both sides of equation (8) as

$$\frac{\partial\tilde{\mathbf{u}}}{\partial m_k} = \mathbf{W}^{-1}\tilde{\mathbf{f}}_k. \tag{18}$$

And $\tilde{\mathbf{f}}_k$ is the virtual source vector (Pratt et al., 1998) of the k^{th} model parameter, which can be written as

$$\tilde{\mathbf{f}}_k = -\frac{\partial\mathbf{W}}{\partial m_k}\tilde{\mathbf{u}}. \tag{19}$$

Substitute equation (18) and (19) into equation (17), we have

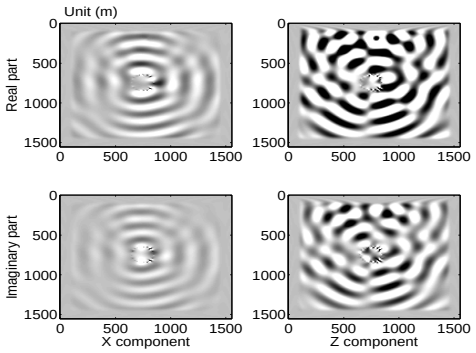

FIG. 1. The wavefields of this true model with a P-wave anomaly in the middle.

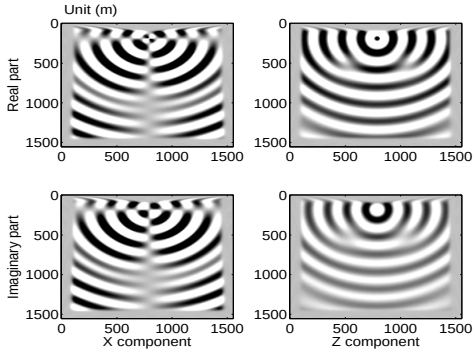

FIG. 2. The wavefields of a homogeneous initial model.

$$\begin{aligned}\nabla_{m_k} E(m_k) &= \sum_\omega \sum_{\mathbf{s}} Re\left[(\tilde{\mathbf{f}}_k)^T (\mathbf{W}^{-1})^T \left(\tilde{\mathbf{u}} - \tilde{\mathbf{d}}\right)^*\right] \\ &= -\sum_\omega \sum_{\mathbf{s}} Re\left[\tilde{\mathbf{u}}^T \frac{\partial \mathbf{W}^T}{\partial m_k} (\mathbf{W}^{-1})^T \left(\tilde{\mathbf{u}} - \tilde{\mathbf{d}}\right)^*\right].\end{aligned} \tag{20}$$

This equation shows the gradient can be built as a product between the incident wavefields $\tilde{\mathbf{u}}$ and the back-propagated wavefields $(\mathbf{W}^{-1})^T \left(\tilde{\mathbf{u}} - \tilde{\mathbf{d}}\right)^*$, with residuals at receiver positions as a back-propagated source. The operator $\frac{\partial \mathbf{W}^T}{\partial m_k}$ with respect to elastic constants in VTI media can be calculated based on equation (11). Take $\frac{\partial \mathbf{W}^T}{\partial c_{11}}$ as an example, it can be expressed as

$$\begin{aligned}\Delta W_{xx}(\mathbf{x},\omega)/\Delta c_{11} &= -\frac{\partial}{\partial x}\frac{\partial}{\partial x} \\ \Delta W_{xz}(\mathbf{x},\omega)/\Delta c_{11} &= 0 \\ \Delta W_{zx}(\mathbf{x},\omega)/\Delta c_{11} &= 0 \\ \Delta W_{zz}(\mathbf{x},\omega)/\Delta c_{11} &= 0\end{aligned} \tag{21}$$

By scaling the gradients of model parameters, the inversion convergence can be accelerated. Considering the computational overburden, the pseudo-Hessian matrix instead of the full Hessian matrix is applied to scale the gradients (Shin et al., 2001). The gradient for each parameter is then calculated using

$$\nabla_{m_k} E(m_k) = \sum_\omega \left(\frac{\sum_{\mathbf{s}} Re\left[(\tilde{\mathbf{f}}_k)^T (\mathbf{W}^{-1})^T \left(\tilde{\mathbf{u}} - \tilde{\mathbf{d}}\right)^*\right]}{\sum_{\mathbf{s}} \left[diag\left((\tilde{\mathbf{f}}_k)^T (\tilde{\mathbf{f}}_k)^*\right) + \lambda \mathbf{I}\right]} \right), \tag{22}$$

in which λ is the damping factor and $\mathbf{I}$ is the identity matrix in Marquardt-Levenberg regularization. We choose $\lambda = 0.01$ in this paper.

Combining all the ingredients, we can calculate the gradients with respect to different

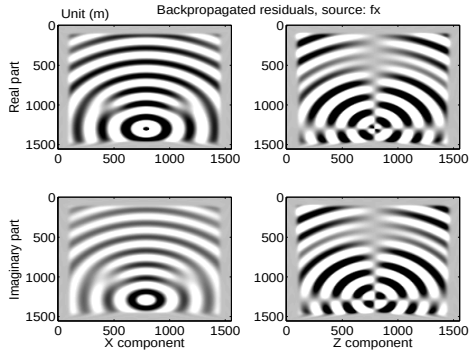

FIG. 3. The wavefields of an X-component back propagated source with a P-wave anomaly in the middle.

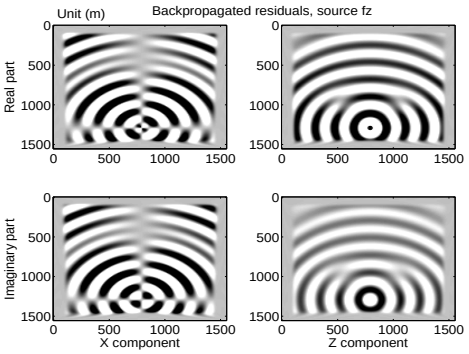

FIG. 4. The wavefields of n Z-component back propagated source in z-direction with a P-wave anomaly in the middle.

parameters. We start from an isotropic model with P- and S-wave velocity of 1500 m/s and 1200 m/s for the background velocities, respectively. A round anomaly (P-wave velocity in this anomaly is 1800 m/s) with a radius of 50 m is located in the middle of the model (the size of the model is $1560 * 1560m^2$, with a PML of $50m$ at each side, the space-sample is $10m$.). A vertical point source S_z is located at $S_z = (200m, 780m)$, and a receiver R is located at $R = (200m, 780m)$. The inverted frequency is 7 Hz. The wavefields of this true model is shown in Figure 1. Take the background without the P-wave velocity anomaly as the initial model, the wavefields wlth respect to x- and z-component can be obtained with the same source-receiver distribution, which are shown in Figure 2. Take the residuals of receivers in both x- and z-components for the true and initial models as sources, the wavefields of horizontal and vertical sources can thus be calculated, shown in Figure 3 and 4. Taking each part as a matrix, the gradient in equation (17) can be written as matrix form

$$\nabla_{m_k} E(m_k) = \left(\begin{bmatrix} \frac{\Delta W_{xx}}{\Delta m_k} & \frac{\Delta W_{xz}}{\Delta m_k} \\ \frac{\Delta W_{zx}}{\Delta m_k} & \frac{\Delta W_{zz}}{\Delta m_k} \end{bmatrix} \begin{bmatrix} \tilde{\mathbf{u}}_x \\ \tilde{\mathbf{u}}_z \end{bmatrix} \right)^T \begin{bmatrix} W_{xx}(\mathbf{x},\omega) & W_{xz}(\mathbf{x},\omega) \\ W_{zx}(\mathbf{x},\omega) & W_{zz}(\mathbf{x},\omega) \end{bmatrix}^{-1} \begin{bmatrix} \tilde{\mathbf{u}}_x - \tilde{\mathbf{d}}_x \\ \tilde{\mathbf{u}}_z - \tilde{\mathbf{d}}_z \end{bmatrix}^* \tag{23}$$

In Figure 5, the gradients of V_P, V_S and $density$ are calculated for this isotropic medium. If we change this isotropic medium into VTI medium, whose stiffness tensor is

$$c_{VTI} = \begin{bmatrix} 23.87 & 9.79 & 0 \\ 9.79 & 15.33 & 0 \\ 0 & 0 & 2.77 \end{bmatrix} \times 10^9 N/m^2, \tag{24}$$

The gradients with respect to different stiffness tensor can also be calculated with equation (21), which are shown in Figure 6.

As an inversion problem, FWI requires intensive computation. An efficient step-length formula is extremely important to accelerate the convergence rate. In this study, we es-

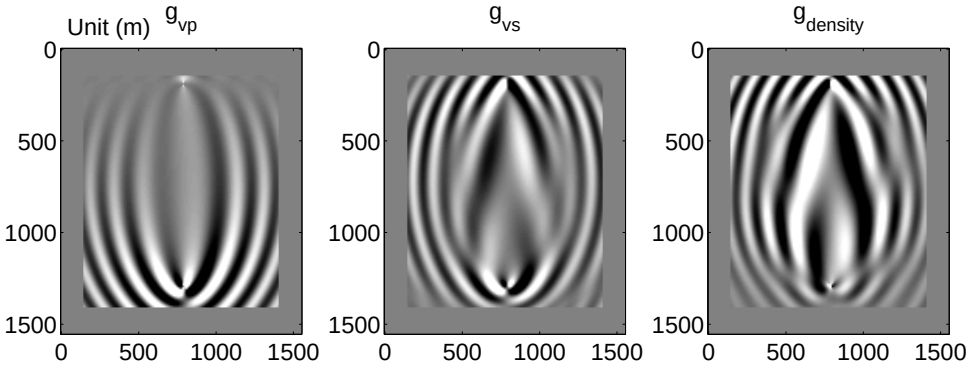

FIG. 5. Sensitivyty kernels for V_P, V_S and density in isotropic media.

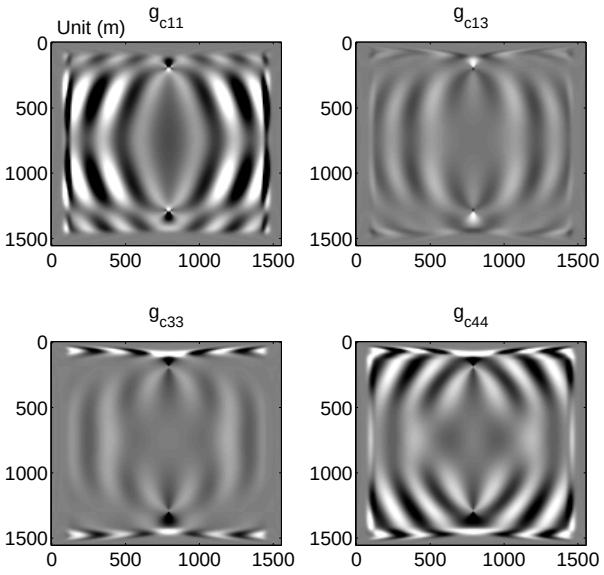

FIG. 6. Sensitivyty kernels for stiffness tensors in VTI media.

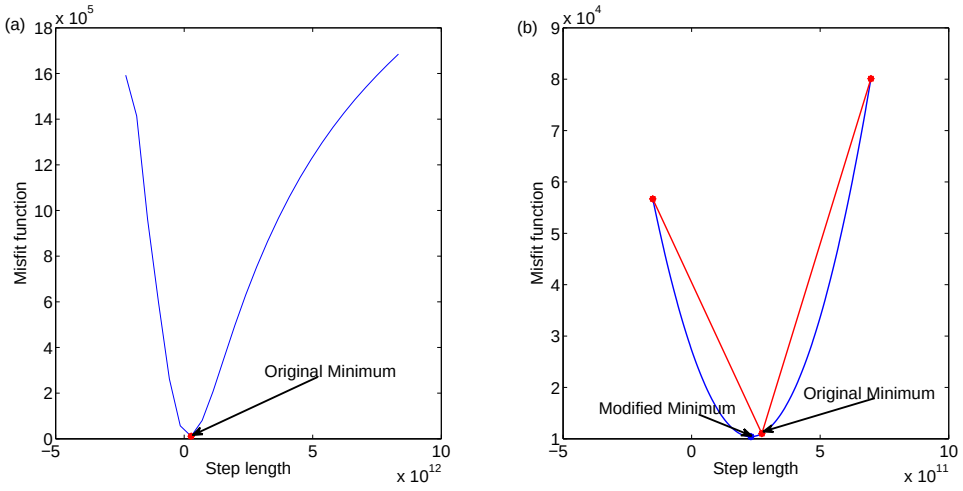

FIG. 7. Illustration that schematically outlines the principle of the modified quadratic interpolation step-length formula. (a) Original step length obtained by line search method and (b) Modified step length after interpolation.

timate the step length by a modified quadratic interpolation method. A step length that minimizes the misfit function can be found by using the line search method, shown in Figure 7(a). Unlike directly using the step length in the iteration, the adjacent left and right closest step lengths are also used (red curve in Figure 7(b)) to interpolate a modified step length that minimizes the misfit function.

EXAMPLES

Two-anomalous model

In this section, a VTI model with two finite-sized anomalous circles of radius 100 m is presented, shown in Figure 8(Left). The background VTI model parameters are the same as in equation (24). The parameter values of the stiffness tensors are increased into 1.4 times of the background parameter values. The stiffness tensor matrix in the anomalies is

$$c_{VTI} = \begin{bmatrix} 33.18 & 13.71 & 0 \\ 13.71 & 21.46 & 0 \\ 0 & 0 & 3.88 \end{bmatrix} \times 10^9 N/m^2, \tag{25}$$

The numerical grid size is 116 by 116 points with a spatial step of 10 m. The source-receiver distribution is shown in Figure 8(Right)(red dots are the receiver locations with a spacing of 20m, the sources are located in the same areas, except the spacing is 50m). We have a total of 54 sources and each source is recorded by 156 geophones located at each side of the model. We choose a start frequency of 2 Hz to 16 Hz with a sample of 2 Hz. The initial medium is the constant background VTI model in equation (24). For each iteration, the updated initial model comes from the previously inverted model with different frequencies.

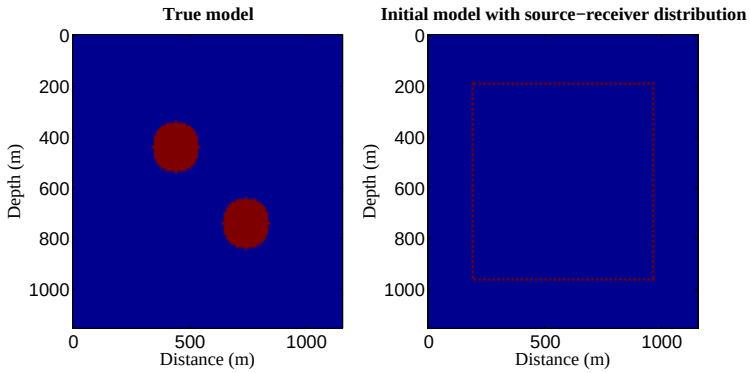

FIG. 8. True model (Left) and initial model with source-receiver distribution (Right).

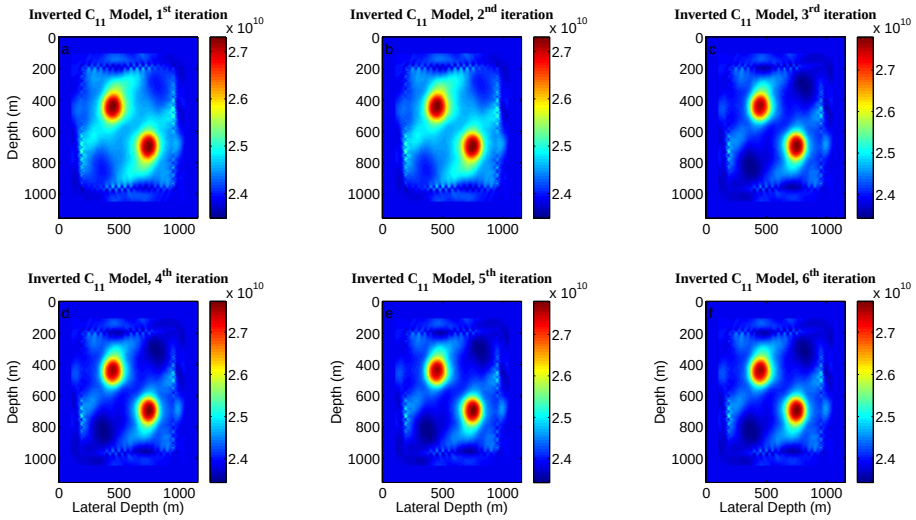

FIG. 9. Inversion results of c_{11} with the increase of iteration steps.

The inversion results of c_{11} and c_{33} are shown in Figure 9 and 10. Both the shape of the anomalies and parameter amplitudes are reconstructed gradually with the increase of iteration times. The inversion results depend on the selected frequencies. The more the inverted frequencies are to be used, the more finely the inversion results would be. It's also obvious that c_{33} converges faster than does c_{11}, as is noticed by Mora (1987) that convergence rate varies between different inverted parameters.

For parameters c_{13} and c_{44}, we also illustrate the inverted results, which are shown in Figure 11. The inverted result of c_{13} contains some noise, but the shape and values of the anomalies are reconstructed. However, for c_{44}, we can not get satisfying result by using the same frequency set. The value of c_{44} in the true model is smaller than the other three parameters, and its perturbation can be neglected compared with those of the other three parameters, which might be a reason for this poor inversion of c_{44}.

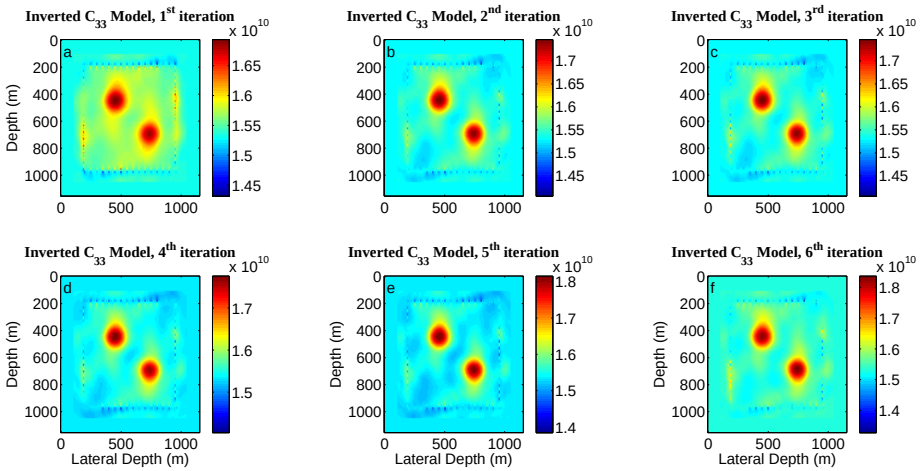

FIG. 10. Inversion results of c_{33} with the increase of iteration steps.

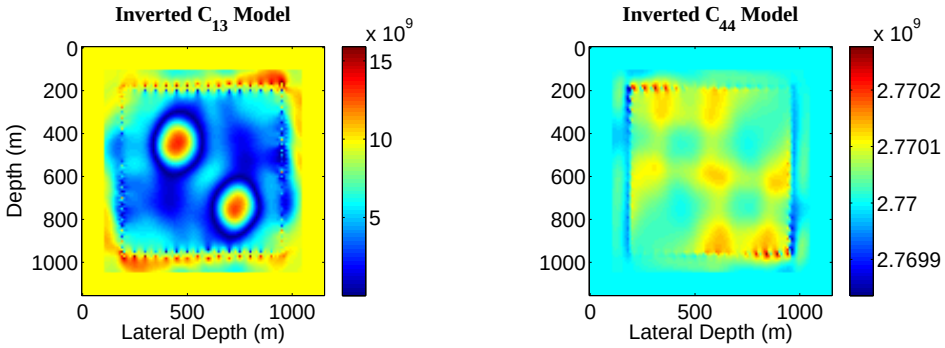

FIG. 11. Inversion results of c_{13} (Left) and c_{44} (Right).

CONCLUSIONS

In this paper, the frequency-domain elastic inversion algorithm for elastic constants in VTI media has been discussed. According to the frequency domain forward modeling, the gradient direction can be easily calculated in forms of matrix multiplication. To accelerate the convergence of inversion, the pseudo-Hessian matrix is applied to constrain the step length. we estimate the step length by a modified quadratic interpolation method. Unlike directly using the step length in the iteration, the adjacent left and right closest step lengths are also used to interpolate a modified step length that minimizes the misfit function. Numerical examples demonstrated that parameters c_{11}, c_{13} and c_{33} can be inverted properly, yet the inversion result of c_{44} is not satisfying.

ACKNOWLEDGMENTS

The authors thank the sponsors of CREWES for continued support. This work was funded by CREWES industrial sponsors and NSERC (Natural Science and Engineering Research Council of Canada) through the grant CRDPJ 461179-13. Author 1 was also supported by SEG scholarship.

REFERENCES

Barnes, C., Charara, M., and Tsuchiya, T., 2008, Feasibility study for an anisotropic full waveform inversion of cross-well seismic data: Geophysical Prospecting, **56**, No. 6, 897–906.

Chang, H., and McMechan, G., 2009, 3d 3-c full-wavefield elastic inversion for estimating anisotropic parameters: A feasibility study with synthetic data: Geophysics, **74**, No. 6, WCC159–WCC175.

Gholami, A., and Siahkoohi, H., 2010, Regularization of linear and non-linear geophysical ill-posed problems with joint sparsity constraints: Geophysical Journal International, **180**, No. 2, 871–882.

Gholami, Y., Brossier, R., Operto, S., Ribodetti, A., and Virieux, J., 2013, Which parameterization is suitable for acoustic vertical transverse isotropic full waveform inversion? part 1: Sensitivity and trade-off analysis: Geophysics.

Kamath, N., and Tsvankin, I., 2016, Elastic full-waveform inversion for vti media: Methodology and sensitivity analysis: Geophysics, **81**, No. 2, C53–C68.

Lailly, P., 1983, The seismic inverse problem as a sequence of before stack migrations.

Lee, H.-Y., Koo, J. M., Min, D.-J., Kwon, B.-D., and Yoo, H. S., 2010, Frequency-domain elastic full waveform inversion for vti media: Geophysical Journal International, **183**, No. 2, 884–904.

Mora, P., 1987, Nonlinear two-dimensional elastic inversion of multioffset seismic data: Geophysics, **52**, No. 9, 1211–1228.

Pan, W., Innanen, K. A., Margrave, G. F., Fehler, M. C., Fang, X., and Li, J., 2016, Estimation of elastic constants for hti media using gauss-newton and full-newton multiparameter full-waveform inversion: Geophysics, **81**, No. 5, R275–R291.

Plessix, R.-É., 2009, Three-dimensional frequency-domain full-waveform inversion with an iterative solver: Geophysics.

Pratt, R. G., Shin, C., and Hick, G., 1998, Gauss–newton and full newton methods in frequency–space seismic waveform inversion: Geophysical Journal International, **133**, No. 2, 341–362.

Pratt, R. G., and Worthington, M., 1988, The application of diffraction tomography to cross-hole seismic data: Geophysics, **53**, No. 10, 1284–1294.

Shin, C., Jang, S., and Min, D.-J., 2001, Improved amplitude preservation for prestack depth migration by inverse scattering theory: Geophysical prospecting, **49**, No. 5, 592–606.

Shin, C., and Min, D.-J., 2006, Waveform inversion using a logarithmic wavefield: Geophysics, **71**, No. 3, R31–R42.

Tarantola, A., 1984, Inversion of seismic reflection data in the acoustic approximation: Geophysics, **49**, No. 8, 1259–1266.

Thomsen, L., 1986, Weak elastic anisotropy: Geophysics, **51**, No. 10, 1954–1966.

Virieux, J., and Operto, S., 2009, An overview of full-waveform inversion in exploration geophysics: Geophysics, **74**, No. 6, WCC1–WCC26.